NASA Technical Memorandum 87328

Thermomechanical Design Criteria for Ceramic-Coated Surfaces

R.L. Mullen
Case Western Reserve University
Cleveland, Ohio

J. Padovan, M.J. Braun, and B.T.F. Chung
University of Akron
Akron, Ohio

G. McDonald and R.C. Hendricks
Lewis Research Center
Cleveland, Ohio

Prepared for the
6th CIMTEC World Congress on High Tech Ceramics,
cosponsored by the Italian Ministry for Science and Technology, the ENEA,
and the American Ceramic Society,
Milan, Italy, June 23–28, 1986

NASA

THERMOMECHANICAL DESIGN CRITERIA FOR CERAMIC-COATED SURFACES

R.L. Mullen
Case Western Reserve University
Dept. of Civil Engineering
Cleveland, Ohio 44106, U.S.A.

J. Padovan, M.J. Braun, and B.T.F. Chung
University of Akron
Dept. of Mechanical Engineering
Akron, Ohio 44325, U.S.A.

G. McDonald and R.C. Hendricks
National Aeronautics and Space Administration
Lewis Research Center
Cleveland, Ohio 44135, U.S.A.

SUMMARY

Some early history of ceramic applications is presented. Finite element modeling of components to determine service and fabrication loads found inelastic behavior and residual stresses to be significant to component life. Inelastic behavior mitigates peak strains but enhances residual strains. Results of furnace, Mach 0.3 burner, and engine tests are discussed and categorized into design criteria (loading, geometry, fabrication, materials, analysis, and testing). These design rules and finite element analyses are brought to bear on two test cases: turboshaft engine seals, and rocket thrust chambers.

E-3002

1. INTRODUCTION

Ceramic coatings on metal substrates have a great potential for reducing heat transfer in engines when the metal-ceramic combination is heated from the ceramic side and cooled from the metal side. The reduced heat transfer permits greater efficiency through the use of higher gas temperature, permits use of less cooling air, or extends component life by reducing metal temperature.

However, serious problems arise in maintaining the integrity of the ceramic coating during use. The ceramic coating can fail from a combination of the stresses resulting from applying the ceramic to the metal and from the expansion of the ceramic-coated metal during use. Tensile loads on a ceramic bonded to a metal substrate simply develop intermittent cracks in the ceramic. Typically the ceramic remains attached to the substrate, at least where the coating is thin enough so that the tensile strength is below the shear strength of the ceramic or the strength of the metal. Increasing the tensile load simply results in closer and closer spacing of the cracks in the ceramic coating. Compressive loads on a ceramic bonded to a metal substrate fail the ceramic catastrophically in large sections by spalling when any compressive stress in the plane of the ceramic coating is large enough so that the component perpendicular to the plane of coating attachment exceeds the coating's strength of attachment to the substrate.

This paper presents discussions of previous experiments and calculations of stresses in ceramic coatings from a number of sources. From the reported behavior, design criteria are established so that a ceramic coating can be made that will accommodate compressive stress without catastrophic failure.

2. EARLY HISTORY

Since antiquity ceramic coatings in the form of porcelain glass have been applied to metal substrates by high-temperature firing. Typically these are bonded to the metal after careful preparation of the metal surface and then formation of some superthin transition bonding medium such as a metal oxide that attaches to both metal and ceramic. Since these porcelain enamels are formed at high temperature, where they are plastic, they are under compression when cooled to ambient temperature because of the difference in thermal expansion between the ceramic and the metal. Care is taken in selecting combinations of metal and porcelain thermal expansion so that the compressive stress on cooling will not be sufficient to spall the ceramic. Additional compressive stress in the ceramic will cause spalling (fig. 1(a)). A net tensile stress in the ceramic will crack the ceramic but will leave it attached (fig. 1(b)).

Porcelain enamels are typically not useful in heat engines because their application to the metal substrates is by melting on or fusion. This means that they soften much below the design use temperature of the metals in heat engines.[1] Therefore heat engines demand a ceramic coating that is at least as refractory as the metal (and preferably more so since the temperature of the ceramic under large ΔT will exceed that of the metal).

In the early 1940's Ernst Schmidt was fabricating ceramic turbine blades for the then-new turbojet engine (ref. 1). The blades were of two basic types: a hollow core with coolant passages, and a membrane over a compliant porous substrate (fig. 2). Apparently Schmidt recognized four basic needs: low thermal conductivity, smooth exterior surface, blade cooling, and strain relief mechanism.

In the late 1950's steel- and copper-heat-sink rocket engine nozzles plasma spray coated with Rokide-A were used in a liquid oxygen-ammonia X-15 engine performance program (ref. 2). Although the engine was cycled from cryogenic temperatures to 4.14 MPa (600 psi) and 2200 °C (4000 °F) in 0.02 sec and ran for 0.2 sec to shutdown, the coatings did not spall but rather eroded away at the throat.

3. CURRENT APPLICATIONS TO HEAT ENGINES

Usually ceramic coatings are applied to metals for heat engines by plasma spraying. To protect the metal in the heat engine from high-temperature oxidation, the metal is conventionally plasma sprayed with NiCrAlY. This material

---

[1]Ceramic softening depends on temperature, heat flux, and local strain rates and may occur in ZrO_2-Y_2O_3 coatings in rocket engine combustion chambers, see also Sections 5 and 6.

is sufficiently oxidation resistant that the formation of oxide is not significant in early failure of ceramic coatings.[2] Typically a coarse NiCrAlY is used so that the sprayed metal is rough; this achieves the second purpose of leaving a surface to which the subsequently plasma-sprayed ceramic mechanically bonds and interlocks.[3]

As in the porcelain enamel (and even more so because the bond strength in plasma-sprayed ceramic is less that in porcelain enamel) the amount of compressive stress in the ceramic on cooling to ambient must be carefully controlled. Although the ceramic is initially plasma sprayed onto a bond-coated substrate at ambient temperature, the ceramic particles are at high temperature as they impact the metal and therefore raise the metal temperature. If the plasma spraying continues long enough without interruption to sufficiently raise the metal temperature, the ceramic will separate from the metal on cooling to ambient.

$$\varepsilon = \frac{\Delta L}{L} = \Delta\alpha \, \Delta T \qquad (1)$$

where ε is strain, ΔL is length, ΔT is the temperature of both metal and ceramic above ambient, and $\Delta\alpha$ the difference in thermal expansion coefficients.

In practice when a metal is plasma sprayed with ZrO_2-$8Y_2O_3$, the metal cannot exceed 300 to 400 °C (570 to 750 °F) for a 0.038-mm (0.015-in.) thick coating without shedding the coating on cooling to ambient.

Applied compressive stress due to differential thermal expansion (using the bulk elastic modulus) is given by

$$\sigma = 7.2\text{x}10^{-6} \text{ x } 400 \text{ x } 3.5\text{x}10^{4} = 100 \text{ MPa } (14.5 \text{ ksi})$$

The compressive stress is applied off axis to the coating in the plane of bonding. The coating is buckled like a thin plate (fig. 3).

The residual compressive stress in the coating from fabrication is additive with any other compressive stresses originating in use. It must be minimized so that the ceramic is under tension when the metal/ceramic returns to ambient. This can be done by slow application of the plasma-sprayed ceramic or by subcooling the metal such as by cooling with liquid nitrogen during ceramic application.

A second stress in the ceramic that is residual from plasma spraying is tensile stress due to differential cooling of the plasma-sprayed particles. The ceramic particle is heated in the plasma jet sufficiently to be plastic.

---

[2]There are at least three time scales associated with plastic, creep, and reactive (e.g., oxidation) strain that may lead to failures.

[3]Mechanical bonding may be improved by hot isostatic pressing (HIP) after plasma spraying (ref. 3). Although HIP improves mechanical bonding, it may lower resistance to spalling by decreasing porosity and increasing compressive stress.

As the particle impacts the solid, it is both rapidly cooled on the side of impact and locked into position on that side. The open side cools more slowly by convection and radiation and flows plastically as it cools to relieve stress until it reaches approximately 1000 °C (1830 °F). Below 1000 °C plastic flow is too little to relieve stress and the thermal contraction from 1000 °C to ambient appears as residual tensile stress. Strain due to thermal contraction[4] is

$$\epsilon = \Delta\alpha\ \Delta T = 8.3\text{x}10^{-6} \times 10^{3} = 8.3\text{x}10^{-3}\ \text{cm/cm}$$

A plasma-sprayed sheet from which the substrate is removed releases the tensile stress by bending the ceramic sheet (fig. 4).

Compressive stress is created in the ceramic when the metal/ceramic combination is heated from the ceramic side. The ceramic is hotter than the metal, and any attempted thermal expansion of the ceramic is resisted by the more massive metal substrate. Ignoring complicating factors, the stress for a rod can be calculated from the heat load Q by

$$\sigma = E\left[\frac{\Delta\alpha\ \Delta T}{2(1 - \upsilon)}\right] \tag{2}$$

where σ is stress, E is Young's modulus, υ is Poisson's ratio, h is thickness, A area, λ thermal conductivity, with $\Delta T = Qh/A\lambda$ and equated to hoop stress

$$\sigma = \frac{Pd}{2h} \tag{3}$$

where P is load/area and d diameter.

4. QUANTITATIVE APPROACH

4.1 Applied-Strain Gas Path Seal Test

Overall the ceramic laminae provide thermal, erosion, and corrosion protection of the substrate metal over a large range of temperatures. Along with the material development studies, complementing analytical work has been performed to determine the potential thermomechanical fields in ceramic coatings under engine operation (refs. 10 to 12). These elastic analyses illustrate the rather severe mechanical fields generated during a typical cycle. Under short-cycle (e.g., 1 min at power, 1 min at idle) operating conditions the composite structure creeps (ref. 7), and this results in severe compressive and tensile stress in the ceramic layers after operation (ref. 11).

---

[4]From bulk ceramic properties the elastic stress is 280 MPa (40 ksi) (refs. 4 to 6). See table I. From the free-form modulus (3400 to 3900 MPa; 500 to 1000 ksi) the elastic stress is 42 MPa (6 ksi) (refs. 7 to 9). These differences are significant and require further verification.

Plasticity effects moderate these stresses during the initial phases of the thermal cycle, but creep effects, which are longer term, do not (refs. 11 and 13).

The thermophysical properties used in the finite element analysis of thermoelastic-plastic creep are functions of temperature. A quasi-static simulation is employed that is transient in temperature and parametrically time dependent in the mechanical fields. For the typical engine thermal cycle the classic Newton-Raphson time-marching algorithm (ref. 14) must be stabilized to yield a converged solution when using a constrained methodology (ref. 15).

4.1.1 Geometry, properties, and environment. - The main thrust of the numerical simulation (e.g., of an outer gas path seal) is to determine creep and plastic straining and to superpose them to yield residual fields.

An outer gas path seal (fig. 5) consists of a superalloy substrate (MAR-M 509) that is coated with three layers of graded zirconia/NiCoCrAlY composite and a fourth layer of yttria-stabilized zirconia (fig. 6). The elastic (Hookean) and thermal (Fourier) properties of the substrate alloy and various ceramic laminae are give in table I.

The thermoelastic-plastic behavior is handled in terms of the usual Von Mises yield surface and strain-hardening flow-rule assumptions. The creep effects are treated in terms of strain-hardening concepts wherein variations in creep rate depend on the existing strain rate. The overall thermoelastic-plastic creep behavior is solved via incremental flow rules. Hence

$$\Delta \underline{S} = (D_{ep})(\Delta \underline{L}_e - \Delta \underline{L}_c - \Delta \underline{L}_T) \tag{4}$$

where D_{ep} is the elastic-plastic material stiffness and $\Delta \underline{S}$, $\Delta \underline{L}_e$, $\Delta \underline{L}_c$, and $\Delta \underline{L}_T$ are, respectively, increments in the second Piola-Kirchoff stress, the Lagrangian strain, and the creep and thermal strains.

If a Prandtl-Reuss relation (ref. 14) is used for computing the requisite creep history, it follows that

$$\Delta \underline{L}_c = \Delta t \, \gamma \underline{S}_d \tag{5}$$

where Δt is an increment in time, $\underline{S}_d$ is the deviatoric stress and

$$\gamma = \frac{\partial \epsilon_{ec}}{\partial t} \frac{1}{\sigma_e} \tag{6}$$

such that σ and $\partial \epsilon_{ec}/\partial t$ are, respectively, the equivalent stress and creep strain rates. The creep behavior of zirconia-based ceramic can be modeled by the relation (ref. 7)

$$\epsilon_{ec} = \begin{cases} A \left[\sigma_e^B \left(\exp \frac{C}{T - T_r} \right) \left(t_p^D \right) \right] & T > T_r \\ 0 & T \le T_r \end{cases} \tag{7}$$

where A, B, C, D, and T_r are empirically obtained correlation parameters. The empirical variable T_r defines the reference temperature at which significant short-term creep strains are initiated in the zirconia-based ceramic.

The increment in thermal strain appearing in equation (4) is defined by the expression

$$\Delta \underline{L}_T = \underline{\alpha}\, \Delta T \tag{8}$$

where $\underline{\alpha}$ is the thermal expansion coefficient matrix and ΔT is the temperature increment. As noted earlier, all material coefficients are temperature dependent.

In the thermal cycle associated with normal seal operation (fig. 7) startup and shutdown are marked by relatively abrupt changes in ambient hot-side operating temperatures.

4.1.2 Thermomechanical field equations. - The quasi-static thermoelastic-plastic creep field equations become (ref. 16)

Thermal:

$$q_{i,j} + Q = \rho C_v T_{,t} \tag{9}$$

$$q_i = -K_{ij} T_{,j} \tag{10}$$

Mechanical

$$[S_{jk}(\delta_{ik} + U_{i,k})]_{,j} + go_i = 0 \tag{11}$$

$$L_{ij} = 0.5\,(U_{i,j} + U_{j,i} + U_{l,j}\, U_{l,i}) \tag{12}$$

where q_i is the heat flux, Q the heat generation (e.g., from a rub), ρ the density, C_v the specific heat, K_{ij} the conductivity tensor, S_{jk} the index form of the second Piola-Kirchoff stress tensor, δ_{ik} the Kronecker delta, U_i the total Lagrangian displacement, go_i the body force, and L_{ij} the index form of the Lagrangian strain tensor.

As a result of temperature-dependent thermophysical properties, creep and plastic strain, and potential kinematic nonlinearities, equations (9) to (12) and their complementing mechanical constitutive relations (eqs. (4) to (7)) are highly nonlinear.

4.1.3 Numerical experiments. - In the finite element mesh used to analyze the thermomechanical fields (fig. 8) eight-noded isoparametric elements were employed. Severe gradients in thermal profiles occurred during both engine warmup and cooldown (figs. 9 and 10).

Ceramic creep did not reduce short-term peak stresses prevalent in the surface laminae and near the ceramic-substrate interface. With increasing time ceramic creep essentially zeroed out the surface stresses in the layers exposed to temperatures over T_r. Upon cooldown creep reversal was typically too short to remove accumulated inelastic strains, and severe residual stresses remained in the surface region.

With plastic creep, peak stresses generated early in the cycle were significantly lower (fig. 11). Essentially the entire layered ceramic coating was plasticized during the initial stages of heating, and strains generated by plasticization dominated those caused by creep effects.

Such inelastic behavior caused significant residual fields after cooldown (figs. 12 and 13). The severest stresses were at the ceramic-substrate interface and were caused by the mismatch in thermal expansion properties. Such stresses can lead to short- as well as long-term delamination.

4.1.4 Significant results. - The quantitative approach yielded the following significant results:

- Severe stresses were generated in the interface zone between the metal substrate and the first ceramic layer.

- Plasticity behavior appeared to dominate creep effects in the ceramic laminae closest to the substrate.

- Plastic and creep effects tended to combine to reduce the surface stress state in the exposed (hot side) ceramic layer.

- Significant residual fields were generated by the inelastic behavior.

4.2 Residual Stress from Plasma Spraying

A large number of studies predict the stress state in a ceramic coating during service loads in a gas turbine engine (refs. 4 to 6, 17, and 18). However, little work has been done to establish the initial stress state in the coating due to the fabrication process. The temperatures, heat fluxes, and thermal strains are not any more severe under service conditions than during plasma spraying. Cooling rates on the order of 10^5 deg K/sec have been reported during the vacuum plasma deposition process (ref. 19).

4.2.1 Finite element model. - The finite element calculations for temperature and stress were performed by using the MARC (ref. 20) program with the two-dimensional bilinear element. The finite element model follows the basic ideas presented by Lee (refs. 21 and 22) to represent the discrete nature of the plasma spraying process. A sequence of problems was solved, each of which represents the addition of one (or a partial) new layer of coating. Since the addition of new regions is not a common feature in a finite element code, the addition of a new layer was modeled by modifying the boundary conditions between each layer to represent the change in contact. All layers were included in the initial calculations, but before it contacted the coating, the ceramic was surrounded by constant-temperature and stress-free boundaries.

4.2.2 Example. - To clarify this procedure, we will examine the deposition of a 0.36-mm (0.014-in.) thick coating in 0.05-mm (0.002-in.) passes. Each layer was represented by 16 elements and assumed to be rectilinear. Initially each block was surrounded by a 1090 °C (2000 °F) gas and was in thermal equilibrium. In the first increment the left side of the first block was connected to an infinite region at 27 °C (80 °F) that represented the substrate. After an interval representing the time between passes, the left side of the second block was connected to the right side of the first block and a single interface temperature was imposed. This procedure was repeated to represent the addition of subsequent layers until the final thickness was achieved.

The stress analysis was done in a similar fashion to the thermal analysis. Before they impacted the coating, the blocks were constrained sufficiently to remove all rigid-body motion. Upon impact these constraints were removed, and the displacements at the interface were unified.

The substrate was modeled as either completely free or completely rigid. The material properties used for the calculations are presented in table I.

The thermal contours just before the impact of the second layer showed an extremely large temperature gradient in the first layer. The thermal contours before the impact of subsequent layers showed that the large thermal gradient continued to exist near the substrate while the rest of the coating remained near the initial temperature of 1090 °C (2000 °F).

These temperature fields were used to set the thermal strain in each layer during impact, but only the final stress field (at room temperature) is presented. The bending stress field when the substrate was assumed to be rigid (fig. 14(a)) shows a large tensile stress at the interface that decreased into the coating. This field would lead to a residual stress field with the opposite sign when compared with the observed tendency of the coating to warp away from the substrate. The bending stress field when the substrate was assumed to be completely flexible (fig. (14(b)) shows a large compressive stress along the interface that became tensile away from the substrate. This result agrees with the observed warping away from the substrate reported in reference 7.

To compare these stress fields with the observed curvature of a ceramic sheet, the equivalent bending moment that results from the stress field in figure 14 was computed.

$$M = \int_{-h/2}^{h/2} x \, dx \tag{13}$$

The resulting bending moment was 0.39 N-m. Using the same material properties and the radius of curvature of the warped sheet (29.7 cm; 11.7 in.) the residual bending moment can be be calculated by

$$M = EIk \tag{14}$$

where E is Young's modulus, I the moment of inerta, and k the curvature. This yields a moment of 0.58 N-m.

4.2.3 Modeling needs. - The finite element model for residual stresses produced by the plasma deposition process can include the effects of layer size and process time as well as nonlinear material behavior. Further work to be done includes the inclusion of convection cooling effects and modeling the void structure by randomly removing elements from the model.

5. DESIGN CRITERIA (RULES OF THUMB)

Most materials presented herein represent the authors' experiences gained from torch and burner rigs, jet and rocket engine tests, and calculations. The subcategories are rather artifical. Even so, the techniques and methods presented can be applied to other ceramic coatings (e.g., porcelain enameling (ref. 1). Furthermore some design problems can be solved by applying methods used with other ceramics or coatings.

5.1 Basic Coating Needs

In protecting surfaces from high heat flux and temperature applications one recognizes six basic needs:

- Low thermal conductivity
- Substrate cooling
- Noncatalytic surfaces
- Strain relief mechanism
- Adhesive/cohesive bonding
- Smooth exterior surface

Although plasma-sprayed ceramics may have low thermal conductivity and be noncatalytic, they lack strain relief mechanisms, possess rough surfaces, and most often are needed where it is difficult to cool the substrate. They also have low adhesive/cohesive strength, and large deviations in the experimentally measured component life imply need to control manufacturing from powder through component testing (ref. 23).

5.2 Loading Considerations

Component life is controlled by thermal cycling rates and time at temperature rather than by thermal level alone (ref. 24) and can be enhanced by controlling the thermal cycle (ref. 25).

In thermomechanical loading, heat flux is as important as temperature (refs. 7, 11, and 13). The heat transfer rates are controlled by the ceramic, the substrate, and the coolant (ref. 6), but in the rocket engine they are also controlled by thermal softening and erosion of the ceramic to the state of equilibrium, after which no further degradation appears to take place (ref. 26).

Component failures occur most often near the bond-coat/ceramic interface (refs. 7 to 13, 23, 24, and 27). Compressive failures are often catastrophic because of the large area exposed when the coating spalls off. Tensile failures usually leave intermittent cracks that tend to close upon cooling. The tensile cracks do not result in immediate loss of the coating but may expedite the onset of other failure modes.

Condensation of salts and oxidation are important in swelling and long-term inelastic effects (refs. 13, 24, and 28). Most salt condensation shortens coating life, in particular that of vanadium (in the form of vanadium pentoxide). Salts are commonly found in fuels (refs. 5 and 28).

Mechanical erosion of ceramic surfaces in a simulated engine environment was carefully studied by Handschuh (ref. 29). Rolls-Royce reports some benefit

of sand inhalation, which provided a glass coating on engine blades for its Saudi Arabian flights (ref. 30).

5.3 Geometry

Plasma-spraying is mostly limited to simple line-of-sight geometries. Internal configurations on the order of 75-mm (3-in.) diameter require special plasma techniques and fixtures. More complex geometries can be made by dissolution of the metallic substrate (ref. 26).

Ceramic coatings 0.19 mm (0.0075 in.) thick on 12.5-mm (0.5-in.) diameter rods in Mach 0.3 burner tests will hang on "forever," and 1-mm (0.040-in.) thick coatings will fall off when they "sniff" the burner (thermocycled to 1030 °C (1900 °F)). Similar results were found for coated 38- by 38-mm (1.5- by 1.5-in.) plates and 25-mm (1-in.) disks (refs. 11, 13, and 24).

Rocket engine thrust chambers with a smooth, thin (0.076 to 0.013 mm; 0.003 to 0.005 in.) ceramic liner can be formed by using the inside-out process (ref. 26).

5.4 Fabrication

Substrate preparation is important. Surfaces are usually cleaned and roughened by grit blasting with Al_2O_3 to mechanically interlock the bond coat. Usually a 0.076 to 0.13 mm (0.003 to 0.005 in.) of bond coat is applied and left rough to assist mechanical interlocking of the plasma-sprayed ceramic. Pinholes in the bond coat provide access for hollowing out (oxidizing) the substrate or bond coat, leaving a fragile ceramic shell (refs. 7, 24, 24, and 31).

The optimum arc current for plasma spraying ceramic may be 650 A, but coating life increases somewhat even to 950 A. Powder size from -200 to +200 mesh is acceptable, but uniform spherical particles may be better (refs. 26, 32, and 33). Furthermore controlling the substrate temperature is necessary, and residual stresses in plasma-sprayed coatings are significant to component life (refs. 18 and 34). Ceramic creep can be controlled by annealing (ref. 9).

Thin ceramic sheets and complex plasma-sprayed free-form shapes can be fabricated by substrate and bond-coat leaching or hot isostatic pressing of greenware. Thin ceramics are compliant and can function as a spring (refs. 7, 26, and 35 to 37).

To some extent the surface texture is controlled by application rates, gun power, and powder (size, shape, and distribution), but it is also controlled by mechanical (grinding) and thermal (laser glazing) means. The inside-out process, which uses either a parting mandrel or leaching out of the mandrel, provides a smooth plasma-sprayed surface (refs. 23, 24, 26, and 31).

Plasma-sprayed coatings can be electroplated as required (ref. 38), and ceramic fibers can be coated with metals and attached to substrates (ref. 39).

5.5 Materials

Plasma-sprayed zirconia stabilized with 7 to 12 percent yttria (YSZ) over a NiCrAlY bond coat provides reasonably good component life (refs. 7, 23, 24, and 26). Plasma-sprayed YSZ creeps to a significant degree above a threshold load (ref. 7) with plastic flow reducing stresses (refs. 13, 18, and 40).

Compressive stresses induce ceramic spalling failures that are catastrophic (ref. 27). High-porosity plasma-sprayed ceramics, ceramic fibers, graded ceramic composites (ref. 12), and a compliant metal matrix (ref. 41) between the ceramic and the substrate are used to provide some strain relief. To resist thermomechanical loadings, high-porosity plasma-sprayed materials are desired. Also fibrous ceramic materials can be coated with metals and bonded; fibrous ceramics arrest cracks (ref. 39). But fibrous materials have poor bond characteristics and poor material strength (ref. 42).

Metals can be electroplated onto and into plasma-sprayed ceramics (ref. 38).

5.6 Analysis and Testing Procedures

Elastic modeling produces unusually high stresses and various codes produce similar results (ref. 10). Heat transfer and mechanical strains (thermomechanical) are nonlinear and are solved in a coupled manner by using finite element codes (e.g., ADINA and ADINAT, ref. 43) (refs. 11, 13, 18, and 40). The problem is complex because ceramic creep reduces strain and substrate/bond-coat plasticity also reduces strain (refs. 7, 10, 11, 13, 18, and 40). Furthermore two- or three-dimensional heat transfer induces additional complications, as has been numerically demonstrated for two-dimensional cylinders in crossflow (ref. 44). Even so, one- and two-dimensional modeling indicates that thermomechanical strains are most significant near the bond-coat/ceramic interface and that there are at least three time scales: plastic, creep, and reactions (oxidation) (refs. 7, 10, 11, 13, and 24).

In a quantitative determination of the influence of bond-coat oxidation on coating life, two series of short-term cyclic heating/cooling tests were conducted with the substrate temperature held constant. In one test the oxygen/fuel ratio (air/propane) was stoichiometric, and in the other it was increased to the flame limits. No appreciable influence on ceramic coating life was found.

High-temperature thermocycled oxidation tests with and without "salt" spray indicated that the NiCrAlY bond coat is extremely resistant to anything other than superficial oxidation. Eventual failure is through a defect that gives rise to pit corrosion, which is followed by rapid degradation in component life. Bond-coat life appears to be an order of magnitude longer that ceramic coating life.

Torch rig tests can be used to simulate engine operations (ref. 45), but heat fluxes must be simulated and component tests must be accrued on a sufficiently large sample set to be meaningful (e.g., ref. 31 ran 1001 cycles and ref. 23 ran sample sets of 20 and 22 specimens).

The log-normal distribution for rod and disk specimens implies decreasing failure function (ref. 23).

Applications to gas path seal engine tests substantiate to some degree the knowledge base (refs. 31 and 46).

6. FABRICATION CONSIDERATIONS

Simple analyses that ignore complicating factors as well as sophisticated finite element analyses show that ceramic coatings on metal substrates fail catastrophically from compressive stresses originating in mechanical or thermomechanical loading. The conclusion to be derived from these analyses is that, if the ceramic coating can be fabricated with a low modulus, it can accommodate and dissipate a compressive strain without developing significant compressive stress. Then a ceramic coating can be manufactured that will withstand large mechanical or thermomechanical loads without catastrophic failure. Two methods of achieving this both produce a segmented ceramic coating:

(1) If the ceramic coating is plasma sprayed onto a supercooled metal substrate, the ceramic upon returning to ambient is under sufficient tensile stress to crack and form separate "tiles." When the ceramic is loaded in compression, no compressive stress develops until the cracks are closed. Plasma spraying the ceramic coating in a vacuum allows the metal substrate to be cooled to, for example, liquid-nitrogen temperatures without condensing gases as water and carbon dioxide.

(2) If the ceramic coating is fabricated in segments, such as with ceramic fibers attached to the metal substrate and oriented perpendicular to the metal surface, the ceramic structure can also accommodate high compressive loads.

7. APPLICATIONS

7.1 Seals

The analysis and design criteria (rules of thumb) were applied to the testing of shroud seals in a turboshaft engine (ref. 31). The bill-of-materiel nickel aluminide seals were replaced with a 1-mm (0.040-in.) thick bond coat and 1-mm-thick ceramic. This is not an optimum configuration, but analysis and tests indicated it would work (fig. 15). The engine was thermal cycled 1001 times, or 57.8 engine hours, which represents a balance between what a pilot might want to see and facility operations time. The thermal cycle consisted of a 1-sec ramp to 80 sec at high power and a 1-sec ramp to 80 sec at low power. Again this was a tradeoff and provided sufficient time at temperature for creep to begin and sufficient coolant time to thermocycle the component. Pre- and post-test micrograph analysis of the seals showed cracks but no evidence of failures (fig. 16). The seals functioned well.

7.2 Thrust Chambers (ref. 26)

The requirement of a smooth surface was satisfied by the inside-out process, where the ceramic is plasma sprayed onto a mandrel with the bond coat sprayed onto the ceramic (fig. 17). The system is then electroplated with copper, machined, and closed out by electroplating. It can then be wound to mitigate hoop stresses. These thrust chambers survived hundreds of hot firings with some coating degradation but without failures (fig. 18).

8. SUMMARY REMARKS

Application of ceramics to heat engines and surfaces is not only useful but will be required to meet future needs. However, the applied and residual strains can be large enough to fail the component. The nonlinear thermomechanical problem with at least three different time scales represents a major challenge, with constitutive relations and thermophysical properties still required. The finite element modeling methodology and rules of thumb presented herein are to assist the designer until such time as the thermomechanical effects can be numerically and experimentally resolved.

9. REFERENCES

1. R.C. Hendricks and G. McDonald, "Some Thermal Stress Problems in Porcelain Enamel Coated Rods," Proceedings of the Porcelain Enamel Institute, Technical Forum, Vol. 42, Porcelain Enamel Institute, Arlington, VA, 1980, pp. 178-187.

2. R.C. Hendricks, R.C. Ehlers, and R.W. Graham, "Evaluation of Injector Principles in a 2400-Pound-Thrust Rocket Engine Using Liquid Oxygen and Liquid Ammonia," NASA Memo 12-11-58E, Jan. 1959.

3. H. Kuribayashi, K. Suganuma, Y. Miyamoto, and M. Koizumi, "Effects of HIP Treatment on Plasma-Sprayed Ceramic Coating onto Metal Substrate," To be published in Am. Ceram. Soc. Bull., 1986.

4. G.S. Simko, B.N. Cassenti, and A.M. Brickley, "JT9D Thermal Barrier Coating Analysis Informal Report," Pratt & Whitney Aircraft Group, PWA-5515-135, Contract NAS3-20630, Sept. 1980.

5. C.A. Andersson, R.J. Bratton, S.K. Lau, S.Y. Lee, J. Allen, K.L. Rieke, and K.E. Munson, "Advanced Ceramic Coating Development for Industrial/Utility Gas Turbines," Westinghouse Electric Corp., Pittsburgh, PA, NASA CR-165619, 1982.

6. C.H. Liebert and F.S. Stepka, "Ceramic Thermal-Barrier Coating for Cooled Turbines," J. Aircr. 14 [5] 487-493 (1977).

7. R.C. Hendricks, G. McDonald, and R.C. Bill, "Some Inelastic Effects of Thermal Cycling on Yttria-Stabilized Zirconia," Ceram. Eng. Sci. Proc., 3 [9-10] 750-757 (1982).

8. R.C. Hendricks, G. McDonald, and R.L. Mullen, "Residual Stress in Plasma Sprayed Ceramic Turbine Tip and Gas Path Seal Specimens," Ceram. Eng. Sci. Proc., 4 [9-10] 802-809 (1983).

9. R.C. Hendricks, G. McDonald, and R.L. Mullen, "The Effect of Annealing on Creep of Plasma Sprayed Ceramics," Ceram. Eng. Sci. Proc., 4 [9-10] 819-827 (1983).

10. R.C. Hendricks, G. McDonald, R.L. Mullen, M.J. Braun, B.T.F. Chung, and J. Padovan, "Thermomechanical Loading of Multilayered Cylindrical Geometries in Thermal Cycling from 300° to 1300° K," ASME/JSME Thermal Engineering Joint Conference, Vol. 3, Edited by Y. Mori and W.J. Yang, ASME, New York, 1983, pp. 329-340.

11. J. Padovan, D. Dougherty, G. McDonald, R. Hendricks, M.J. Braun, and B.T.F. Chung, "High Temperature Thermomechanical Analysis of Ceramic Coatings," J. Thermal Stress, 7 [1] 51-74 (1984).

12. C. Taylor and R.C. Bill, "Thermal Stresses in a Plasma-Sprayed Ceramic Gas Path Seal," J. Aircr., 16, [4] 239-246 (1979).

13. J. Padovan, B.T.F. Chung, M.J. Braun, R.L. Mullen, R.C. Hendricks, and G. McDonald, "Application of a Plastic Flow Thermomechanical Algorithm to Plasma-Sprayed Ceramic Turbine Seals," Presented at 9th Annual Conference on Composites and Advanced Ceramic Materials, Cocoa Beach, FL., Jan. 20-24, 1985.

14. J. Padovan and S. Tovichakchaikul, "On the Solution of Creep Induced Buckling in General Structure," Comput. Struct., 15 [4] 379-392 (1982).

15. J. Padovan and T. Arechaga, "Formal Convergence Characteristics of Elliptically Constrained Incremental Newton-Raphson Algorithms," Int. J. Eng. Sci., 20 [10] 1077-1099 (1982).

16. Y.C. Fung, Foundations of Solid Mechanics, Prentice Hall, NJ, 1965.

17. E.B. Shand, Glass Engineering Handbook, 2nd ed., McGraw-Hill, 1958.

18. J. Padovan, G. McDonald, R.C. Hendricks, R.L. Mullen, B.T.F. Chung, and M.J. Braun, "Plastic Flow of Plasma Sprayed Ceramics," Plastic Deformation of Ceramic Materials II, Edited by R.E. Tressler and R.C. Bradt, Plenum Press, New York, 1984, pp. 473-485.

19. H.A. Davies, "Rapid Quenching Techniques and Formation of Metallic Glasses," Rapidly Quenched Metals III, Vol. 1, Edited by B. Cantor, Metals Society, London, 1978, pp. 1-21.

20. MARC J2 Users Manual, MARC Analysis Research Corporation, Palo Alto, CA, 1983.

21. L. Daeyong, "A Finite Element Modeling of the Low Pressure Plasma Deposition Process. I-Temperature Analysis," Int. J. Mech. Sci., 25 [8] 543-551 (1983).

22. L. Daeyong, "A Finite Element Modeling of the Low Pressure Plasma Deposition Process. II-Stress Analysis," Int. J. Mech. Sci., 25, [8] 553-563 (1983).

23. R.C. Hendricks and G. McDonald, "The Assessment of the Variations in Thermal Cycle Life Data of Thermal Barrier Coated Rods," NASA TM-81743, 1981.

24. G.E. McDonald, and R.C. Hendricks, "Effect of Thermal Cycling on ZrO_2-Y_2O_3 Thermal Barrier Coatings," Thin Solid Films, 73 491-496 (1980).

25. R.C. Hendricks, G. McDonald, and N.P. Poolos, "Prolonging Thermal Barrier Coated Specimen Life by Effective Thermal Cycle Management," NASA TM-81742, 1981.

26. R.J. Quentmeyer, G. McDonald, and R.C. Hendricks, "Fabrication of Ceramic Substrate Reinforced and Free Forms by Mandrel Plasma Spraying Metal Ceramic Composites," J. Vac. Sci. Technol. A, 3 [6] 2450-2455 (1985).

27. R.L. Mullen, G. McDonald, R.C. Hendricks, and M.L. Hofle, "Correlation of Compressive and Shear Stress with Spalling of Plasma Sprayed Ceramic Materials," Ceram. Eng. Sci. Proc., 4 [9-10] 810-818 (1983).

28. R.A. Miller, "Oxidation-Based Model for Thermal Barrier Coating Life," J. Am. Ceram. Soc., 67 [8] 517-521 (1984).

29. R.F. Handschuh, "High-Temperature Erosion of Plasma-Sprayed, Yttria-Stabilized Zirconia in a Simulated Turbine Environment," AIAA Paper 85-1219, July 1985.

30. F.C. Toriz, "Communication at Coatings Forum - 12th International Conference on Metallurgical Coatings, Am. Vacuum Soc., Los Angeles, CA. Apr. 15-19, 1985.

31. T.J. Biesiadny, G.A. Klann, E.S. Lassow, M. McHenry, G. McDonald, and R.C. Hendricks, "Experimental and Analytical Study of Ceramic Seals for Turbojet Engines," Ceram. Eng. Sci. Proc., 6 [7-8] 880-895 (1985).

32. R.C. Hendricks and G. McDonald, "Effects of Arc Current on the Life in Burner-Rig Thermal Cycling of Plasma Sprayed ZrO_2-Y_2O_3," Ceram. Eng. Sci. Proc., 3 [9-10] 737-743 (1982).

33. K.T. Scott, and J.L. Woodhead, "Gel-Processed Powders for Plasma Spraying," Thin Solid Films, 95 219-225 (1982).

34. R.L. Mullen, R.C. Hendricks, and G. McDonald, "Finite Element Analysis of Residual Stress in Plasma-Sprayed Ceramic," Ceram. Eng. Sci. Proc., 6 [7-8] 871-879 (1985).

35. R.C. Hendricks, G. McDonald, and R.L. Mullen, "A Technique to Fabricate Complex Free Form Ceramic Components," Presented at the Gas Path Rub Energetics Workshop, NASA Lewis Research Center, Cleveland, OH, Dec. 8-9, 1983.

36. R.L. Mullen, and C. Scavuzzo, "Fabrication and Analysis of High Temperature Ceramic Free Form Static Seals," Presented at the 8th Annual Conference on Composites and Advanced Ceramic Materials, Cocoa Beach, FL, Jan. 15-20, 1984.

37. K.T. Scott, "Ceramic Coatings for Engineering Applications," Materials for the Process Industries, Institute of Mechanical Engineers (1982), pp. 99-106.

38. R.C. Hendricks, G. McDonald, and R.L. Mullen, "Film and Interstitial Formation of Metals in Plasma-Sprayed Ceramics," J. Vac. Sci. Technol. A, 3 [6] 2456-2458 (1985).

39. R.C. Hendricks and G. McDonald, "Summary Abstract: Metallic and Metallo-Ceramic Coating by Thermal Decomposition," J. Vac. Sci. Technol. A, 3 [6] 2655-2656 (1985).

40. J. Padovan, B.T.F. Chung, M.J. Braun, and R.L. Mullen, "An Improved Plastic Flow Thermomechanical Algorithm and Heat Transfer Analysis for Plasma Sprayed Ceramics," Presented at the 8th Annual Conference on Composites and Advanced Ceramic Materials, American Ceramic Society, Cocoa Beach, FL, Jan. 15-20, 1984.

41. R.P. Tolokan, J.B. Brady, and G.P. Jarrabet, "Strain Isolated Ceramic Coatings for Gas Turbine Engines," ASME Paper 85-GT-96, Mar. 1985.

42. R.C. Hendricks and G. McDonald, "Use of Fiber Like Materials to Augment Cycle Life of Thick, Thermoprotective-Seal Coatings," Ceram. Eng. Sci. Proc., 3 [9-10] 744-749 (1982).

43. K.J. Bathe, "ADINA: A Finite Element Program for Automatic Dynamic Incremental Nonlinear Analysis," Report No. 82448-1; and "ADINAT: A Finite Element Program for Automatic Dynamic Incremental Nonlinear Analysis of Temperatures," Report No. 82448-5, Acoustics and Vibration Lab, Dept. of Mechanical Engineering, Massachusetts Institute of Technology, 1978.

44. B.T.F. Chung, M.M. Kermani, M.J. Braun, J. Padovan, G. McDonald, and R.C. Hendricks, "Heat Transfer in Thermal Barrier Coated Rods with Circumferential and Radial Temperature Gradients," J. Eng. Gas Turbines Power, 107 [1] 135-141 (1985).

45. J.K. Little, G.P. Allen, G. McDonald, and R.C. Hendricks, "Ribbon-Burner Simulation of T-700 Turbine Shroud for Ceramic Lined Seals Research," Ceram. Eng. Sci. Proc., 6 [7-8] 849-861 (1985).

46. G. McDonald, R.C. Hendricks, T.J. Biesiadny, and J.K. Little, "Experimental and Analytical Study of Ceramic Seals for Turbojet Engines," Presented at 9th Annual Conference on Composites and Advanced Materials, Cocoa Beach, FL, Jan. 20-24, 1985.

TABLE I. - MATERIAL PROPERTIES USED IN CALCULATIONS[a]

Property	YSZ/CoCrAlY, percent				
	100/0	84/15	70/30	40/60	MAR-M 50
	Material set				
	1	2	3	4	5
Density, lb/in.^{3} [b]	0.155	0.180	0.205	0.254	0.320
Poisson's ratio[b]	0.25	0.26	0.27	0.28	0.30
Thermal conductivity, Btu/min in. °F:					
At 0 °F	4.09×10^{-4}	4.09×10^{-4}	4.09×10^{-4}	4.09×10^{-4}	422.98×10^{-4}
At 200 °F	4.09×10^{-4}	4.09×10^{-4}	4.09×10^{-4}	4.09×10^{-4}	422.98×10^{-4}
At 500 °F	4.09×10^{-4}	4.66×10^{-4}	4.98×10^{-4}	5.38×10^{-4}	422.98×10^{-4}
At 1000 °F	4.33×10^{-4}	6.26×10^{-4}	7.46×10^{-4}	8.35×10^{-4}	422.98×10^{-4}
At 1500 °F	4.74×10^{-4}	8.51×10^{-4}	10.60×10^{-4}	12.20×10^{-4}	422.98×10^{-4}
At 2000 °F	5.70×10^{-4}	11.64×10^{-4}	14.85×10^{-4}	17.66×10^{-4}	422.98×10^{-4}
At 2500 °F	8.11×10^{-4}	16.30×10^{-4}	20.95×10^{-4}	25.52×10^{-4}	422.98×10^{-4}
Specific heat, Btu/lb °F:					
At 0 °F	0.126	0.121	0.116	0.107	0.097
At 2500 °F	0.161	0.161	0.161	0.158	0.155
Coefficient of expansion, in./in. °F:					
At 0 °F	4.08×10^{-6}	3.28×10^{-6}	3.36×10^{-6}	3.64×10^{-6}	6.40×10^{-6}
At 2500 °F	4.83×10^{-6}	7.70×10^{-6}	8.38×10^{-6}	9.52×10^{-6}	12.20×10^{-6}
Young's modulus, lb/in.^{2}:					
At 0 °F	6.90×10^{6}	3.80×10^{6}	5.15×10^{6}	8.30×10^{6}	34.70×10^{6}
At 2500 °F	2.00×10^{6}	2.00×10^{6}	8.00×10^{6}	17.75×10^{6}	15.60×10^{6}
Tensile strength, lb/in.^{2}:					
At 0 °F	4.25×10^{3}	6.00×10^{3}	8.10×10^{3}	33.25×10^{3}	40.0×10^{3}
At 2500 °F	3.30×10^{3}	7.25×10^{3}	11.75×10^{3}	1.00×10^{3}	40.0×10^{3}

[a]From refs. 12 and 44.
[b]For all test temperatures (0, 200, 500, 1000, 1500, 2000, and 2500 °F).

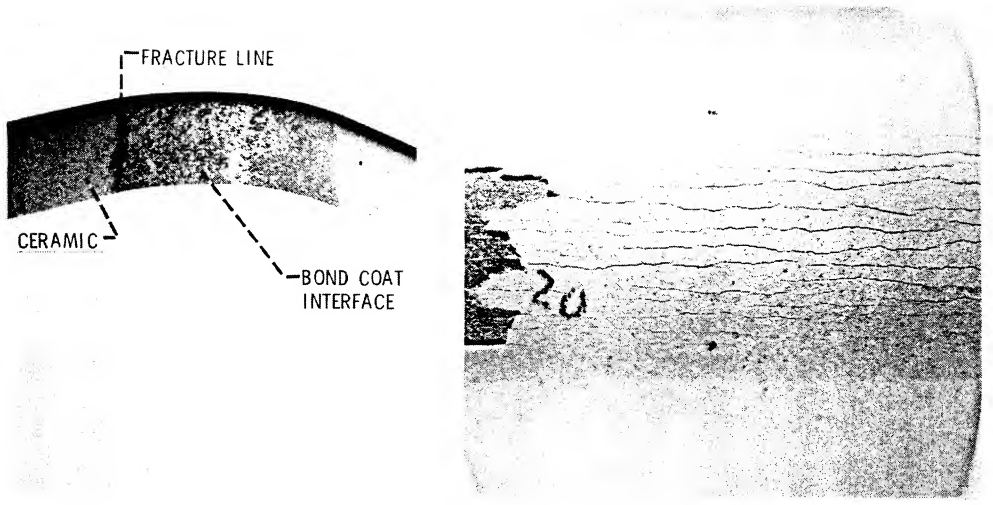

(a) Compression. (b) Tension. t = 0.51 mm (0.020 in.)

Figure 1. - Flexure failure of ceramic coatings.

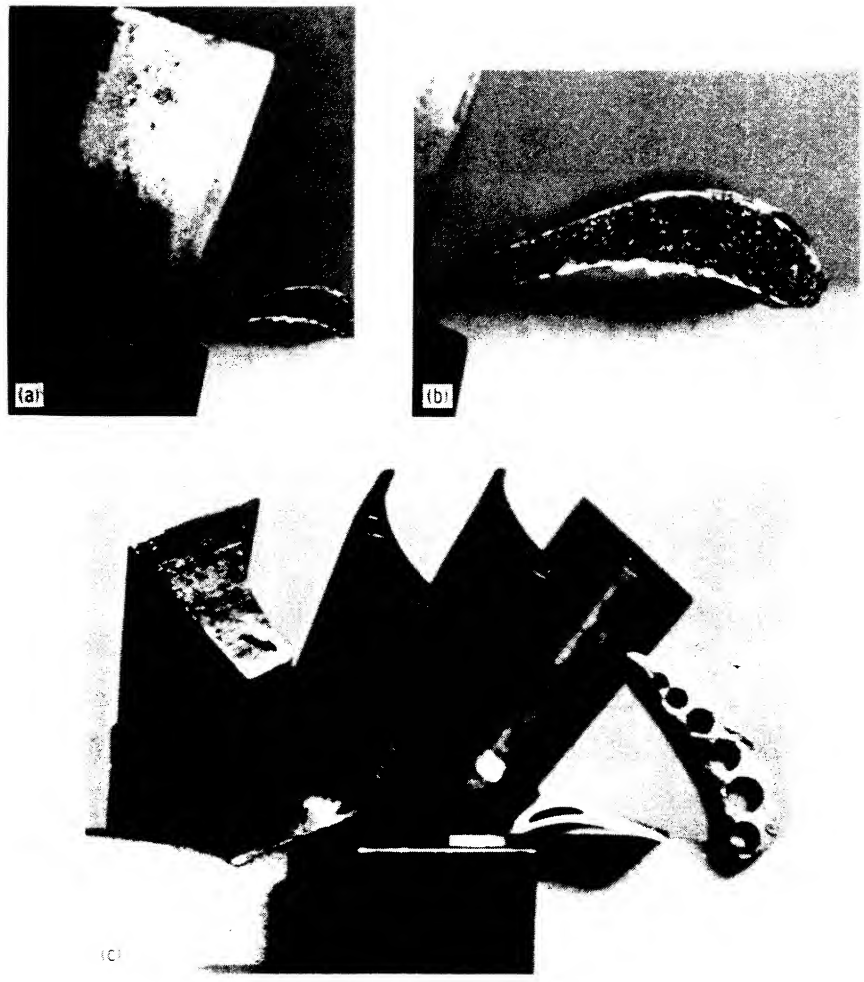

Figure 2. - Prof. Schmidt's experimental ceramic vanes and blades.

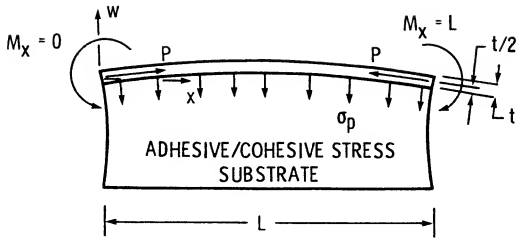

Figure 3. - Ceramic buckling and shear failure.

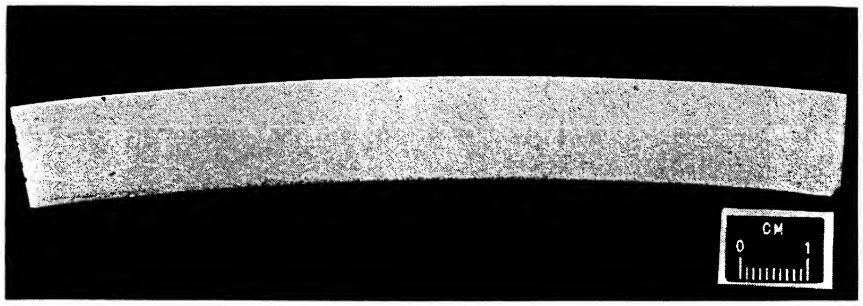

Figure 4. - Ceramic stripped by acid dissolution.

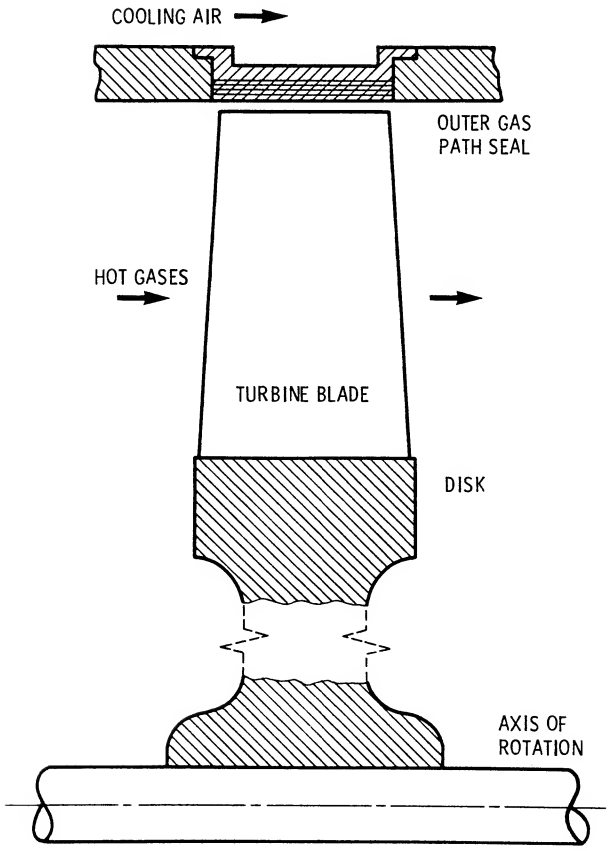

Figure 5. - Cross section of gas turbine.

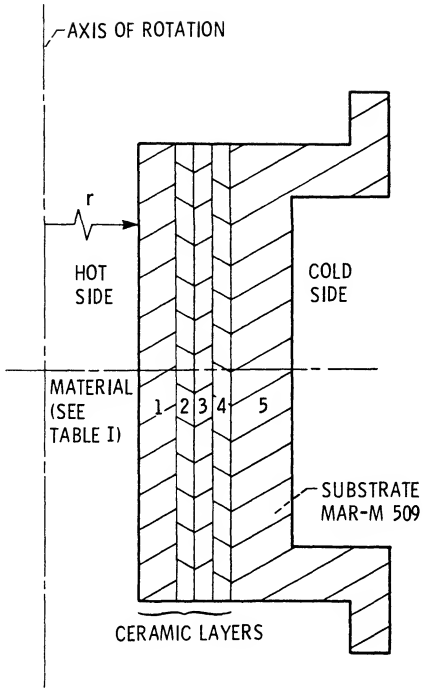

Figure 6. - Outer gas path seal.

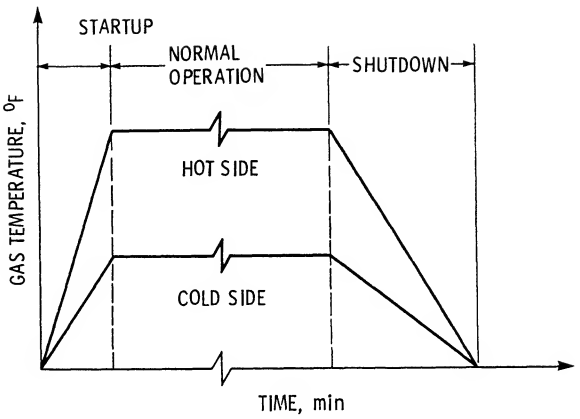

Figure 7. - Hot- and cold-side gas temperature cycle.

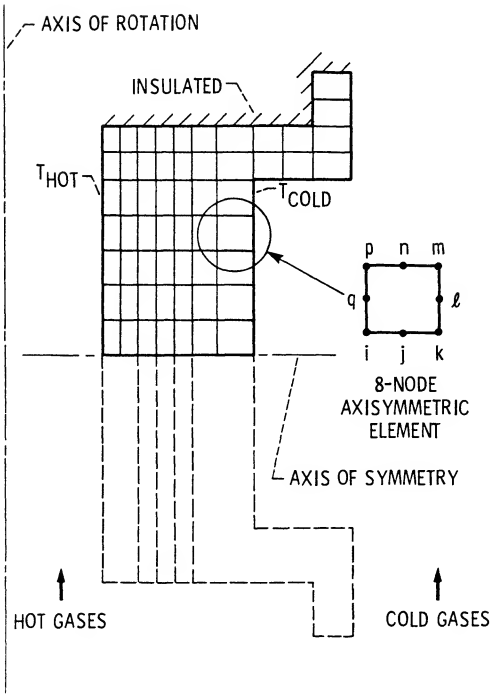

Figure 8. - Finite element simulation of seal.

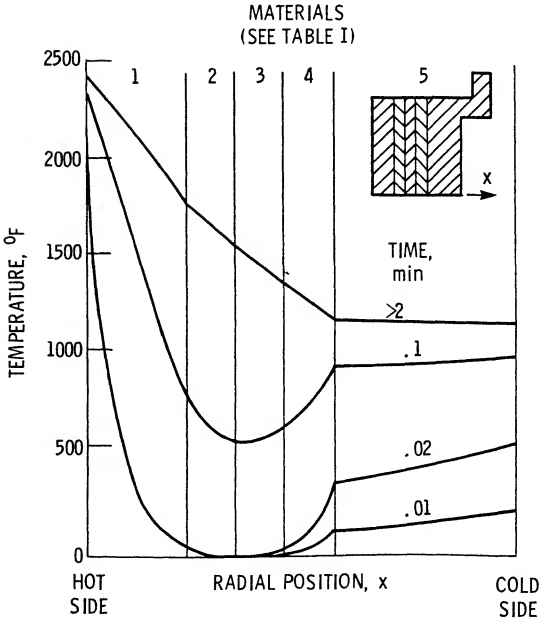

Figure 9. - Warmup temperature profiles.

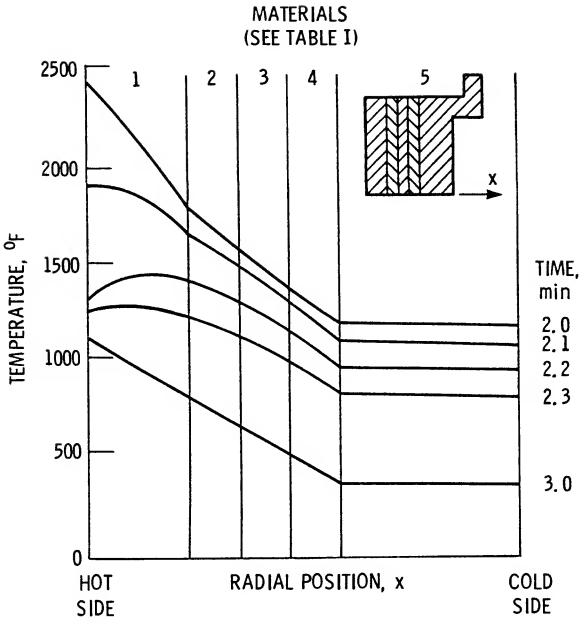

Figure 10. - Cooldown temperature profiles.

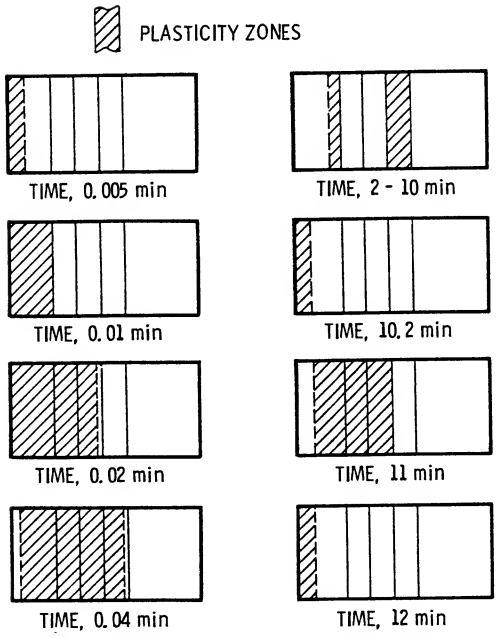

Figure 11. - Growth and subsidence of plasticized zones during thermal cycle.

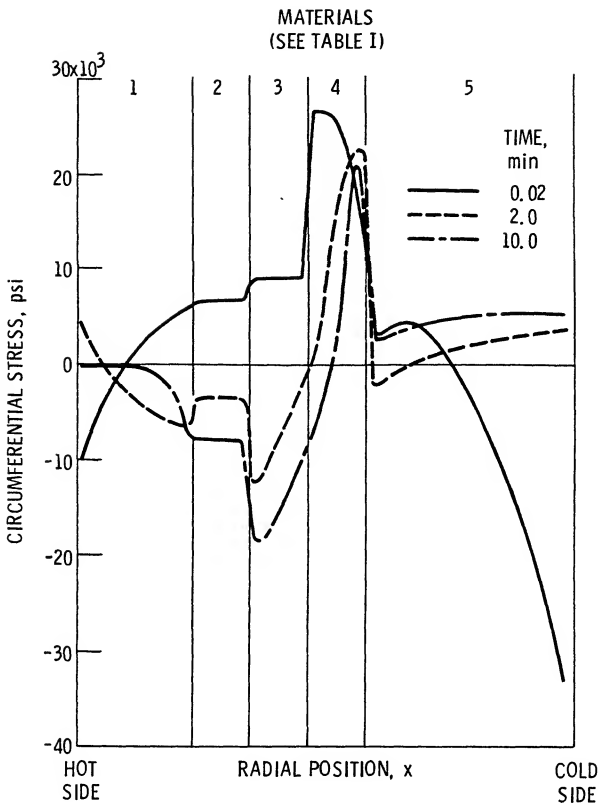

Figure 12. - Stress state of cross-sectional field during heatup.

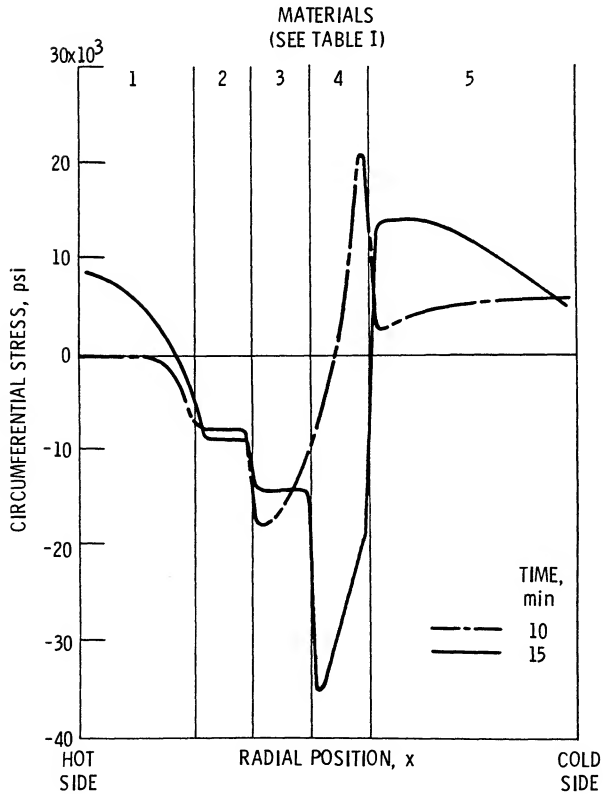

Figure 13. - Stress state of cross-sectional field during cooldown.

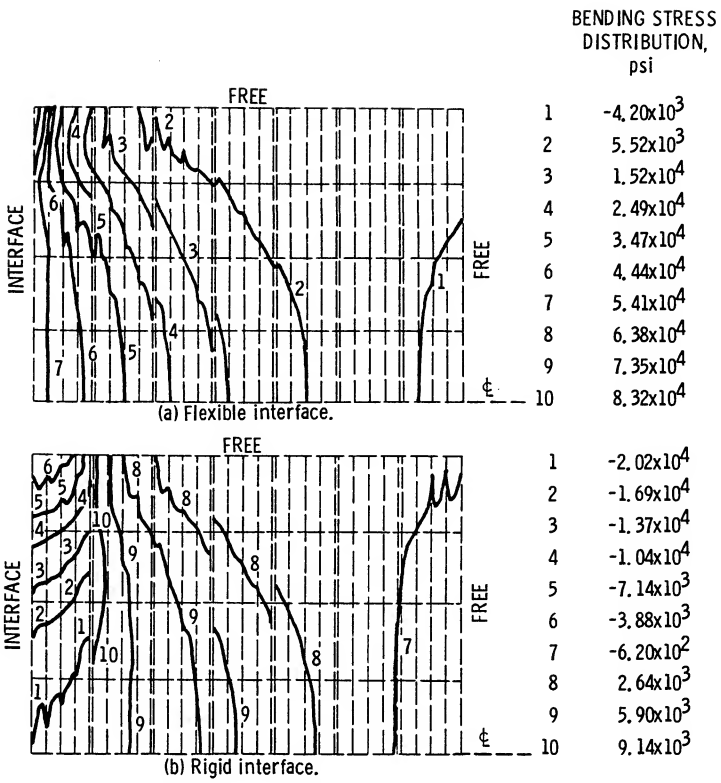

Figure 14. - Bending stress distribution in a 0.36-mm-thick ceramic coating.

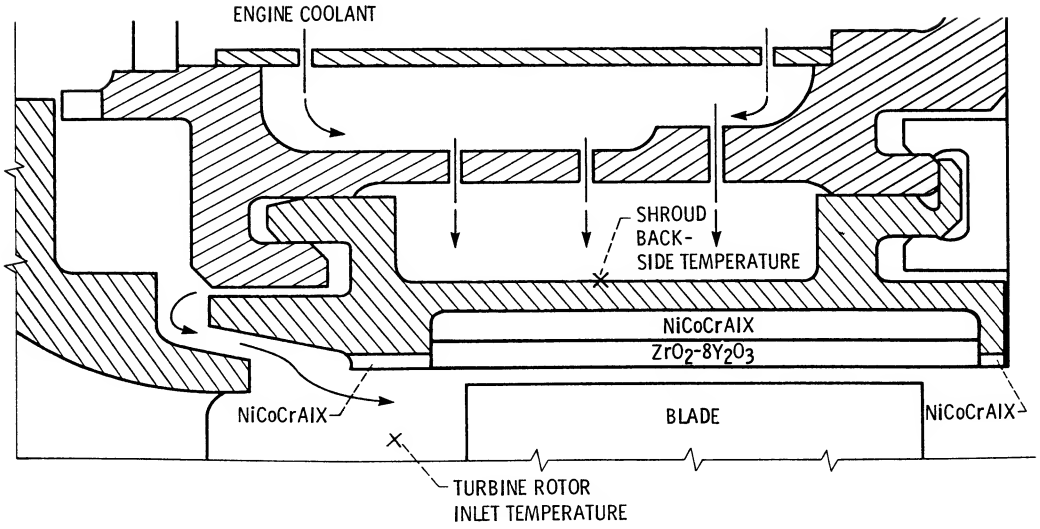

Figure 15. - Schematic of ceramic-coated shroud seal.

ERRATA

NASA Technical Memorandum 87328

THERMOMECHANICAL DESIGN CRITERIA FOR CERAMIC-COATED SURFACES

R.L. Mullen, J. Padovan, M.J. Braun, B.T.F. Chung,
G. McDonald, and R.C. Hendricks

June 1986

Figure 14 should be replaced with the attached copy of that figure.

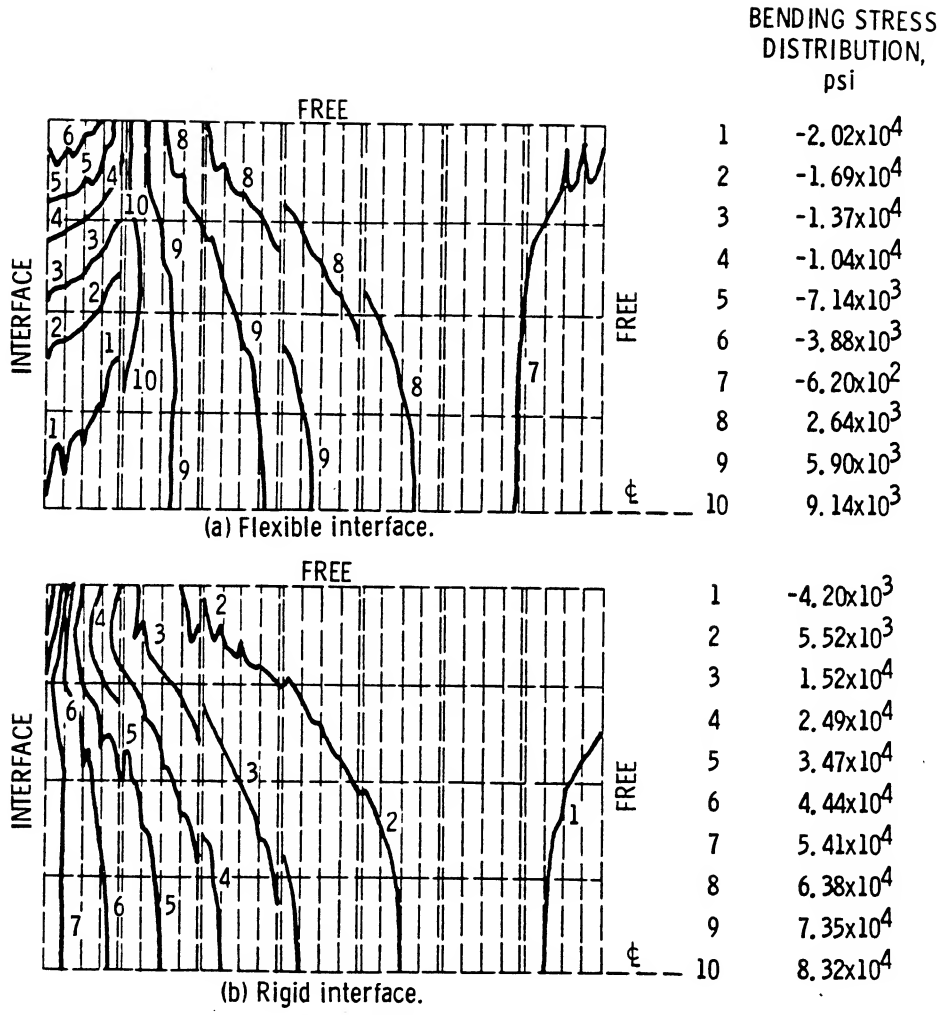

Figure 14. - Bending stress distribution in a 0.36-mm-thick ceramic coating.

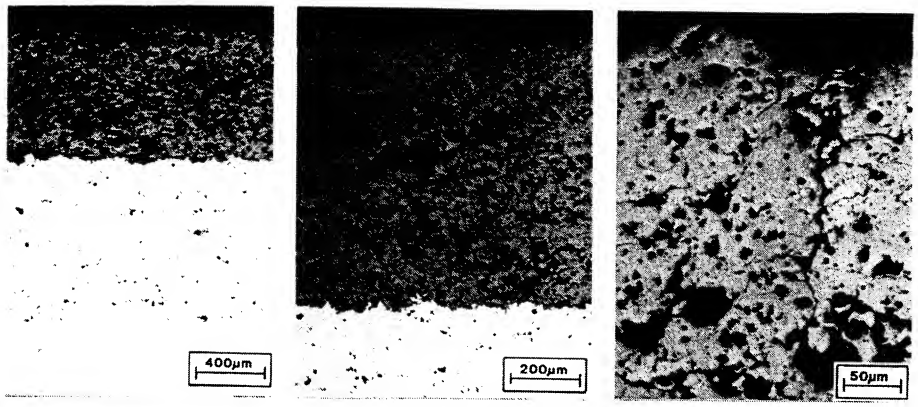

(a) Pretest microstructure across center of shroud segment.

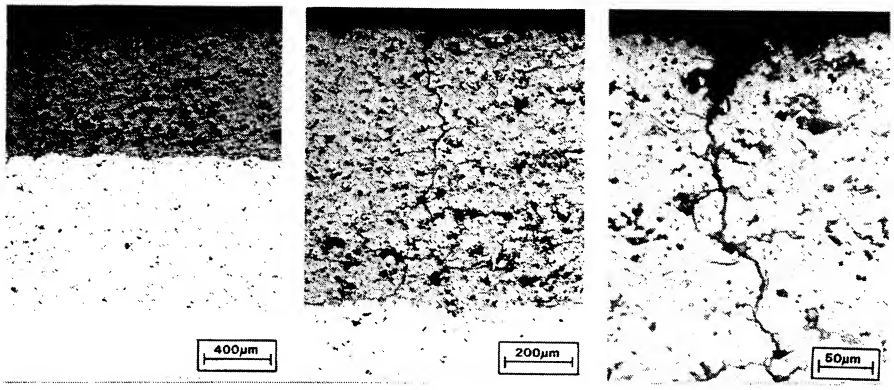

(b) Post-test microstructure across end of shroud segment.

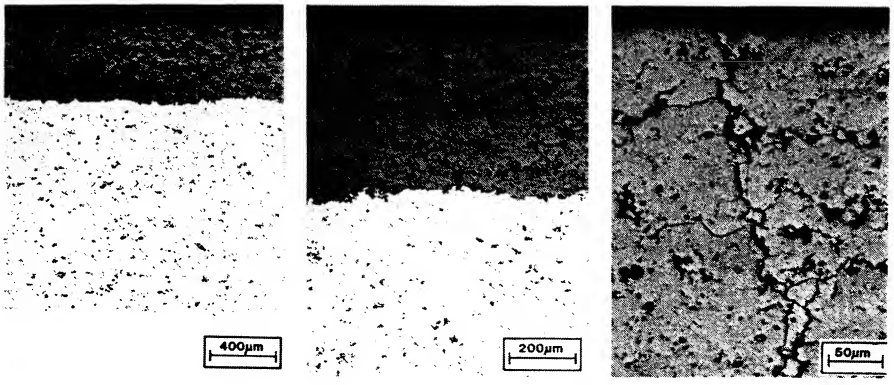

(c) Post-test microstructure across center of shroud segment.

Figure 16. - Plasma-sprayed Zr_2-$8Y_{203}$/NiCoCrAlX/ Haynes 25 shroud.

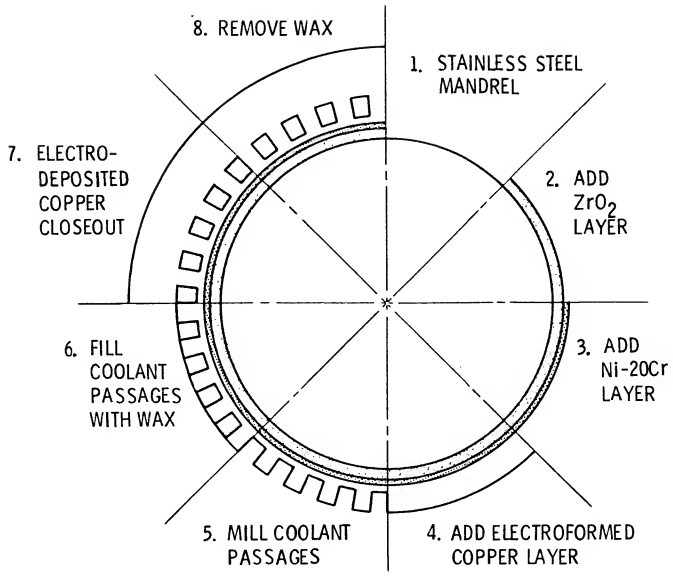

Figure 17. - Inside-out fabrication sequence for ceramic-lined thrust chambers.

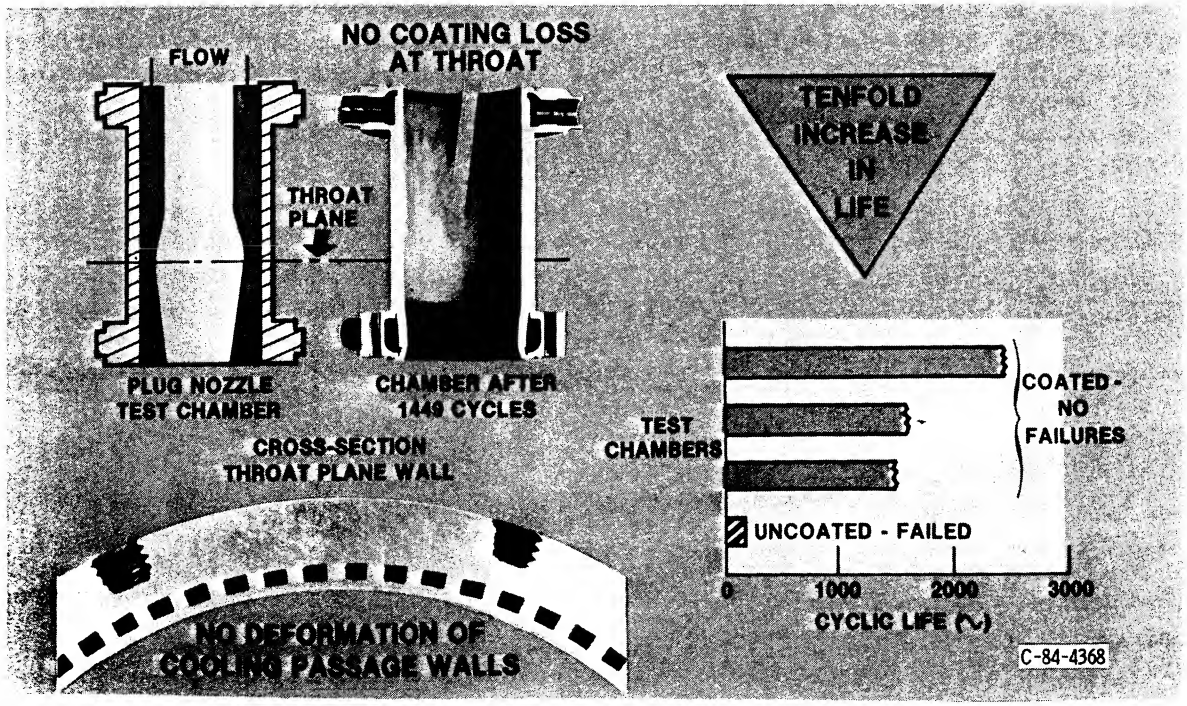

Figure 18. - Cycle life increase of ceramic-lined rocket engine thrust chambers over uncoated chambers.

1. Report No.	2. Government Accession No.	3. Recipient's Catalog No.
NASA TM-87328		

4. Title and Subtitle	5. Report Date
Thermomechanical Design Criteria for Ceramic-Coated Surfaces	6. Performing Organization Code: 505-62-22

7. Author(s)	8. Performing Organization Report No.
R.L. Mullen, J. Padovan, M.J. Braun, B.T.F. Chung, G. McDonald, and R.C. Hendricks	E-3002
	10. Work Unit No.

9. Performing Organization Name and Address	11. Contract or Grant No.
National Aeronautics and Space Administration Lewis Research Center Cleveland, Ohio 44135	13. Type of Report and Period Covered: Technical Memorandum

12. Sponsoring Agency Name and Address	14. Sponsoring Agency Code
National Aeronautics and Space Administration Washington, D.C. 20546	

15. Supplementary Notes

Prepared for the 6th CIMTEC World Congress on High Tech Ceramics, cosponsored by the Italian Ministry for Science and Technology, the ENEA, and the American Ceramic Society, Milan, Italy, June 23-28, 1986. R.L. Mullen, Case Western Reserve University, Dept. of Civil Engineering, Cleveland, Ohio 44106, U.S.A.; J. Padovan, M.J. Braun, and B.T.F. Chung, University of Akron, Dept. of Mechanical Engineering, Akron, Ohio 44325, U.S.A.; G. McDonald and R.C. Hendricks, NASA Lewis Research Center.

16. Abstract

Some early history of ceramic applications is presented. Finite element modeling of components to determine service and fabrication loads found inelastic behavior and residual stresses to be significant to component life. Inelastic behavior mitigates peak strains but enhances residual strains. Results of furnace, Mach 0.3 burner, and engine tests are discussed and categorized into design criteria (loading, geometry, fabrication, materials, analysis, and testing). These design rules and finite element analyses are brought to bear on two test cases: turbo-shaft engine seals, and rocket thrust chambers.

17. Key Words (Suggested by Author(s))	18. Distribution Statement
Ceramics; Coatings; Thermomechanical; Stress; Design criteria	Unclassified - unlimited STAR Category 34

19. Security Classif. (of this report)	20. Security Classif. (of this page)	21. No. of pages	22. Price*
Unclassified	Unclassified		

*For sale by the National Technical Information Service, Springfield, Virginia 22161